Malaysian Journal of Chemistry, 2025, Vol. 27(3), 543-556
(Special Issue: *International Conference on Sustainable Materials and Technologies, ICSMT 2025*)

Metallurgical Bonding, Interfacial Chemistry, and Mechanical Optimization of Dissimilar AA7079–AA6063 Welds via Response Surface Methodology

Mohankumar, K.[1], Pugazhenthi, R.[2]*, Ajith Arul Daniel[3], Sreeram, D.[4], Vamsi Krishna Mamidi[5] and Pavan Kishore, M. L.[6]

[1]Engineering Department, University of Technology and Applied Sciences, Ibra Sultanate of Oman
[2,3]Department of Mechanical Engineering, VISTAS, Chennai, India
[4]AWH Engineering College, Kozhikode, Kerala, India
[5]Department of Mechanical Engineering, SV College of Engineering, Tirupati, India
[6]Department of Mechanical Engineering, Faculty of Science and Technology, ICFAI Foundation for Higher Education, Hyderabad, Telangana, India
*Corresponding author (e-mail: pugal4@gmail.com)

This paper aims at establishing the best FSW process parameters during joining AA 7079 and AA 6063 to achieve the strong joint with good mechanical properties. The experiment design used the Taguchi L9 orthogonal array to investigate the FSW parameters of tool rotation speed, axial force, and welding speed. Nine different sets of parameters were used to produce the FSW joints were made, percentage elongation, hardness value, tensile strength and impact strength of the weld joints were studied. The response surface methodology (RSM) is used to find out the interaction between the process factors and mechanical properties. The RSM analysis helps analyze and find the best welding conditions for the AA 7079 with AA 6063. The investigation of the mechanical properties obtained from the joints prepared with the optimized parameters have shown closer agreement with the RSM model thus signifying the potential of this approach in improvement of mechanical properties of dissimilar AA 7079-AA 6063 FSW joints.

Keywords: FSW; AA 7079; AA 6063; dissimilar material; RSM; optimization

Received: February 2025; Accepted: May 2025

Dissimilar materials are made up of two or more materials that, when their qualities are combined, function as a single entity. Other materials are regarded as reinforcement, while the bulk elements serve as a matrix. Predicting the characteristics of a metal matrix composite is challenging. Among various several metal joining friction stir welding process is one of the pioneer method, which is used to combine stainless steel, copper, titanium, magnesium, and aluminum combinations. The solid-state joining method called friction stir welding has gained significant attention for its impressive capability to bond different aluminum alloys. This technique proves to be incredibly useful in industries such as aerospace and automotive, where the demand for high-performance aluminum joints is crucial. Compared to conventional welding techniques, FSW has advantages such as lower energy consumption and no hazardous emissions. Optimizing process parameters, comprehending joint features, and investigating novel approaches to improve weld quality and mechanical qualities are the main goals of the research on FSW of dissimilar aluminum alloys. The method works well for combining plates and sheets, but it can also be used for positional welding, pipelines, and hollow sections [1-3]. Low melting alloys, which are challenging to combine with traditional fusion welding, may benefit from the procedure. Due to their special properties; low melting point, high strength to weight ratio, low density, high ductility, good corrosion resisting properties, adequate cryogenic properties, non-magnetic properties, easy working, easy machining properties, it is necessary to pay some special attention to the aluminum alloys in this respect. When using Al alloy solutions and performing fusion welding, the occurrences of voids, hot cracking, distortion of shape, precipitate resolution, and loss of work hardening are the results [4].

Various distinct aluminum alloy combinations have been effectively friction stir welded, achieving superior joint efficiency. In the majority of these studies, considerable mechanical amalgamation of the two alloys were identified in the stir zone or weld-nugget, exhibiting intricate vortex, whorl, and swirl characteristics indicative of chaotic-dynamic mixing [5-6]. 5083 and 6061 AA via FSW are studied by Shige Matsu et al. 7. Through this research, he explained, a tool moves along the plates and creates a zone that is highly permanently linked. Friction between the tool and the upper portion of the plate and permanent joints combined with the tool created the local zone [7-8]. To enhance the quality of the joint,

†Paper presented at the International Conference on Sustainable Materials and Technologies (ICSMT 2025)

improvements in FSW technology have focused on modifications of the tool geometry, process parameters, and post-weld treatments of the joint. The flow and intermixing of materials, affected by the geometry of the tool, traverse speed, and rotational speed, are important factors of FSW in different alloys 8, 9. The emergence of intermetallic compounds (IMCs) at the interface of FSW joints has been observed to greatly impact mechanical characteristics for the worse, especially for aluminum-copper alloys. Although FSW is capable of making joints without defects for some material combinations such as aluminum and steel, the creation of brittle Fe-Al intermetallic phases is problematic [9-10].

In magnesium-aluminum alloys, while FSW improves microstructures, the Mg-Al intermetallic can weaken the joint. There has been some focus recently on the novel approaches to overcome these difficulties in dissimilar alloy FSW. To control thermal cycling and prevent brittle intermetallic growth, some hybrid approaches of FSW have introduced controlled heating and cooling features [11]. For example, some intermetallic layers of the resulting joints were found to be thinner due to the cooling rate being increased, thereby making the joint stronger. Tool design is important as well. research done on tools comparing different geometries of pin tool boxes showed that tapered, threaded pins are less defective and better at mixing the materials than traditional cylindrical ones [12]. Furthermore, aluminum-steel FSW has been reported to have improved joint performance with less tool wear when using TiN coated WC tools. The incorporation of PCBN and composite materials also improves the tool life and joint performance significantly [13].

Post-weld heat treatment (PWHT) is turning into a critical procedure for improving the efficiency of FSW joints in the form of different alloys [14]. Some research on titanum-aluminium joints reveals that PWHT helps to dissolve brittle intermetallic as well as replenishes microstructural elements, which subsequently increases strength and ductility. As well, investigation of magnesium-aluminum FSW joints showed that PWHT greatly enhances the fatigue life of the joint by relieving residual stresses and distributing microstructures more evenly. All these results demonstrate the need for proper coordination of thermal management, tool development, and post-processing for effective joining of dissimilar materials by FSW [15].

Analyzing the impact of FSW variables on the weldability of metals is a crucial step forward in the study of aluminum alloy weldability. This evaluation showed how Response Surface Methodology (RSM) played a key role in determining the optimal tool rotation and traverse speed settings, which are vital for producing welds with the best mechanical properties and impeccable quality [16]. Research has shown that Response Surface Methodology (RSM) can lead to impressive outcomes by fine-tuning Friction Stir Welding (FSW) parameters to boost joint strength. By employing RSM, researchers were able to optimize various factors in their investigation of dissimilar welding between AA6061 and AA7050 alloys, ultimately resulting in improved ultimate tensile strength and hardness levels [17]. The research shows that Response Surface Methodology (RSM) plays a crucial role in optimizing Friction Stir Welding (FSW) parameters for different alloys when used together [18-19]. This systematic approach enables scientists to create reliable predictive models by analyzing adjustable parameters, leading to improved welds with better mechanical properties [20-22].

This research work aimed to explore the operational parameters of FS welding for joining dissimilar aluminum alloys AA 7079 with AA 6063. The research team investigated the role of TRS, AF and WS in shaping the mechanical qualities of welded joints assessed through tensile strength evaluations as well as percentage of elongation assessments and impact strength observations and hardness value measurements [23-25]. In this research investigation Taguchi's L9 orthogonal array with RSM, which is used to identify superior parameter sets which lead to optimal mechanical properties of the FSW joint [26]. The mathematical is developed with prediction model assists industrial applications by determining FSW joint mechanical performance from process parameters to refine welding techniques and expand the FSW range for dissimilar aluminum alloy applications [27-29].

EXPERIMENTAL STUDY

Materials

The AA7079 and AA6063 Hybrid Composite aluminum alloys are produced before the friction stir welding procedure. In this investigation, 100 mm x 50 mm x 3 mm plates were utilized 20, and as seen in Fig. 2, they were fastened firmly to the patronage to the plates for welding. The chemical compositions of the two Alloys of Al (AA7079 and AA6063) used in this study have high difference as they made for use with different applications. The composition of AA7079 consists mainly of zinc (5.1–6.1%), magnesium (2.1–2.9%), and copper (1.2–2.0%) as major alloying components supplemented by nutty chromium (0.18–0.28%). Contractively, AA6063 has considerably less zinc (≤ 0.10%) and copper (≤ 0.10%) within it, yet again with moderate magnesium (0.45–0.9%) and silicon (0.2–0.6%) as its leading alloying alloys [30-32]. For both alloys, there are very few amounts of iron (≤ 0.50% AA7079 ≤ 0.35% AA6063), manganese (≤ 0.30% AA7079 ≤ 0.10% AA6063), and titanium (≤ 0.20% AA7079, ≤ 0.10% AA6063) with aluminum representing the remainder in each case. Retry Claude can make mistakes. Please double-check responses.

Experimental Setup

The two dissimilar aluminium alloy plates made of aluminum alloy were fastened together. As seen in Fig. 1, the experimentation was set up in the milling machine used for FSW. The plain cylindrical tool is used for FSW process the H13 steel is used as a tool material. The tool was machined to make to provide a machining tool with a diameter of 20mm rod in H13 tool materials using a lathe to specifications 21. The LMW KODI-40 vertical milling machine is used to join the dissimilar AA 7079 with AA 6063 aluminum alloy plates. The FSW process involved a non-consumable plain cylindrical tool made up of H13 steel with a TRS of 1000 rpm applying an AF of 4 kN with a WS of 30 mm/min. The dissimilar aluminum workpieces in order not to move the pieces during the welding procedure. During its operation, the turning H13 steel tool was stabbed into the region between the plates of aluminum alloy until the shoulder made contact with the surface of the workpiece, producing high levels of frictional heat. Metal plasticism was achieved by the phosphoryl chloride/thermal energy/mechanical stirring combination in a plasticized area where the material flow did not reach the melting point, thus enabling solid-state joining of the different aluminum alloys. The obtained butt joint demonstrated high mechanical properties, which were tensile strength 123.45 MPa, elongation 10.35%, impact strength 20 Joules, microhardness 110.4HV. The mechanical properties are a direct indicator of success of the chosen processing parameters in achieving a metallurgical bond of sound qualities, with refined grain structure, and with minimum defects in the stir zone.

A key factor in figuring out the mechanical characteristics of materials is the apparatus used to measure tensile and impact strengths. The main tool for evaluating tensile strength is the Universal Testing Machine (UTM), which measures elongation and tensile strength by applying a uniaxial force to a specimen until it breaks 22. The ASTM Standards E8 is followed in tensile testing, the tensile specimen are shown in Figure 2.

Figure 1. FSW Setup.

Figure 2. Tensile strength Specimens.

Figure 3. Impact Strength Specimens.

The most popular piece of equipment for determining impact strength is the Impact Testing Machine, which comes with Charpy and Izod testers 23. ASTM E23 standard provide the protocols for notched bar impact testing are followed in impact testing, the after tested impact strength are shown in Figure 3.

RSM ANALYSIS OF AA 7079 WITH AA 6063

The variables taken into account for the dissimilar aluminum alloys 6063 and 7079 that were fused using a triangle tool during the FSW procedure. In accordance with the Taguchi L9 orthogonal array, nine specimens in total were produced by adjusting parameters such Tool Axial Force (AF), Welding Speed (WA), and Rotational Speed (TRS). Through the application of RSM analysis, the ideal set of input parameters was found 24. The variables and reactions of AA 7079 FS welded with AA 6063 are presented in table 1 and the table 2 shows the L9 orthogonal Array with output parameters.

Table 1. Factors of AA 7079 FS welded with AA 6063**.**

Factor	Name	Units	Minimum	Maximum
TRS	Tool Rotational Speed	(rpm)	1000.00	1200.00
AF	Axial Force	(kN)	4.00	6.00
WS	Welding Speed	(mm/min)	30.00	60.00

Table 2. L9 orthogonal Array with output Parameters.

S. No.	TRS (rpm)	AF (kN)	WS (mm/min)	Tensile Strength (MPa)	Elongation (%)	Impact Strength (Joules)	Micro Hardness
1	1000	4	30	123.45	10.35	20	110.4
2	1000	5	45	126.98	11.54	24	129.1
3	1000	6	60	132.35	11.26	20	124.3
4	1100	4	45	136.42	12.21	24	130.2
5	1100	5	60	135.67	11.28	23	117.8
6	1100	6	30	110.64	10.04	21	120.8
7	1200	4	60	129.68	10.26	22	118.4
8	1200	5	30	138.42	14.62	19	129.2
9	1200	6	45	137.46	11.24	20	108.2

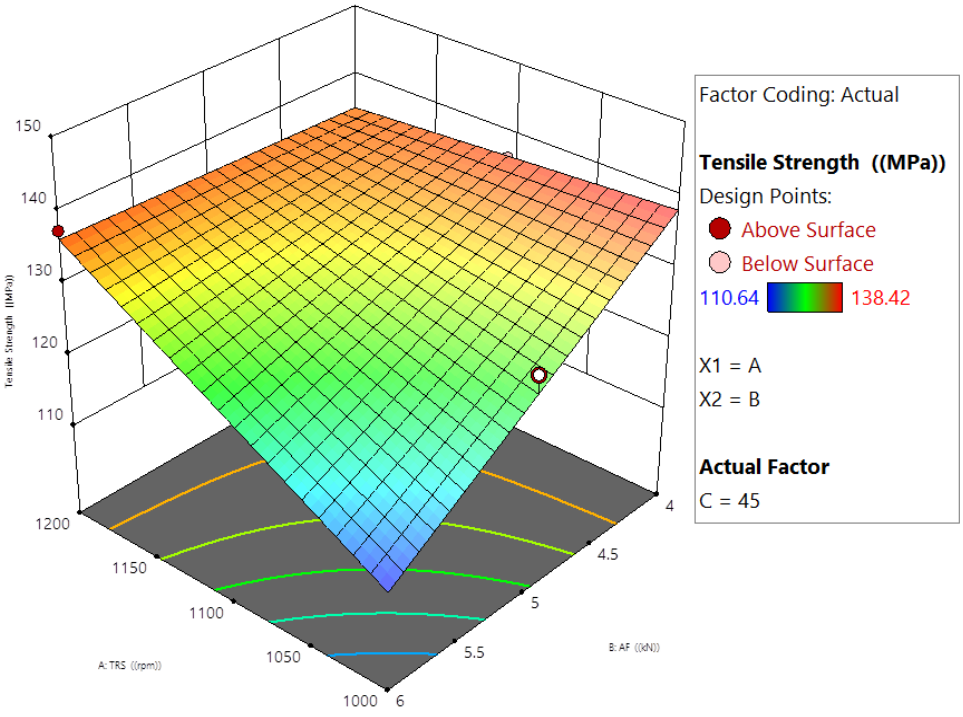

Figure 4(a). 3D surface plot between Tensile Strength, Axial Force and TRS.

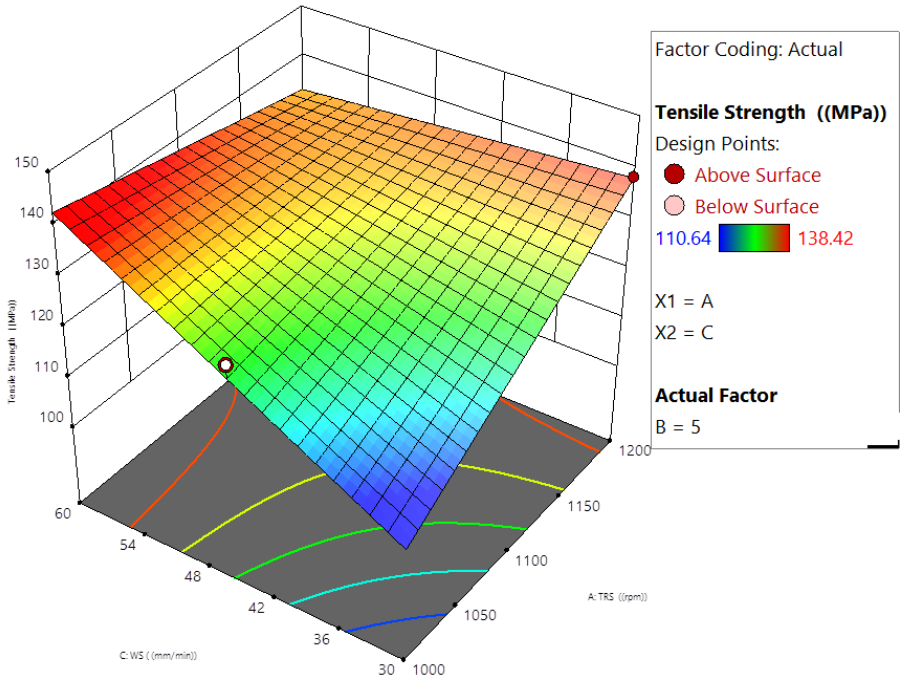

Figure 4(b). 3D surface plot between Tensile Strength, Welding speed and TRS.

RESULT AND DISCUSSION

The Figure 4a Illustrate the 3D surface plot that demonstrates an analysis utilizing RSM to examine the tensile strength measured in MPa. The investigation focuses on two factors, namely X1 (A-TRS, ranging between 1000 to 1200 rpm) and X2 (C-WS, ranging from 30 to 60 mm/min). It constitutes a fundamental element of a RSM analysis directed towards the optimization of parameters concerning the friction stir welding of AA 6063 and 7079. Reaching a Tool Rotational Speed (TRS) nearing 1200 rpm with a

notable Axial Force (AF) of approximately 6 kN results in the highest tensile strength. In contrast, the minimum tensile strength is recorded at low TRS values coupled with moderate to high axial force levels. A consistent improvement in tensile strength is evident with the increase in both TRS and AF.

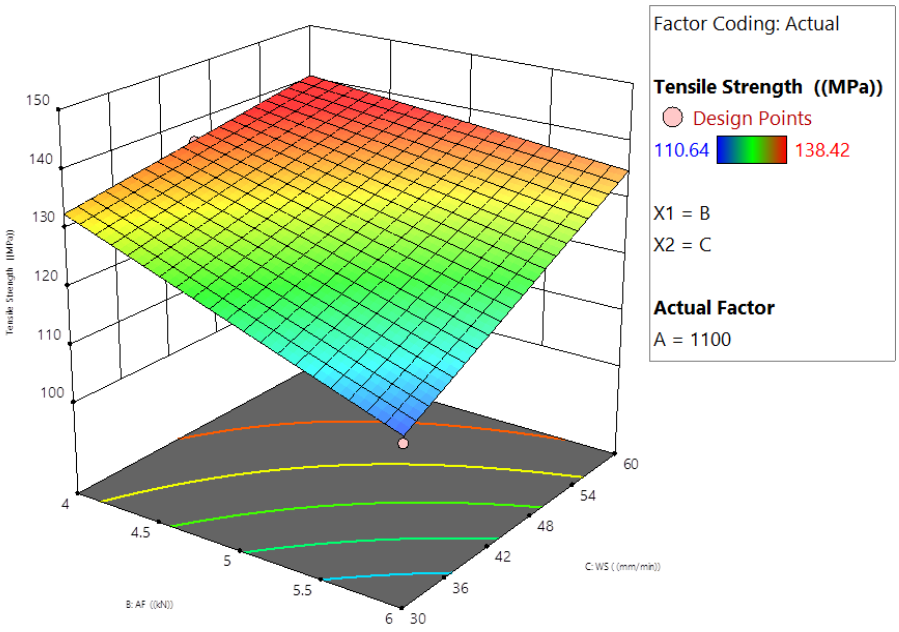

Figure 4(c). 3D surface plot between Tensile Strength, AF and WS.

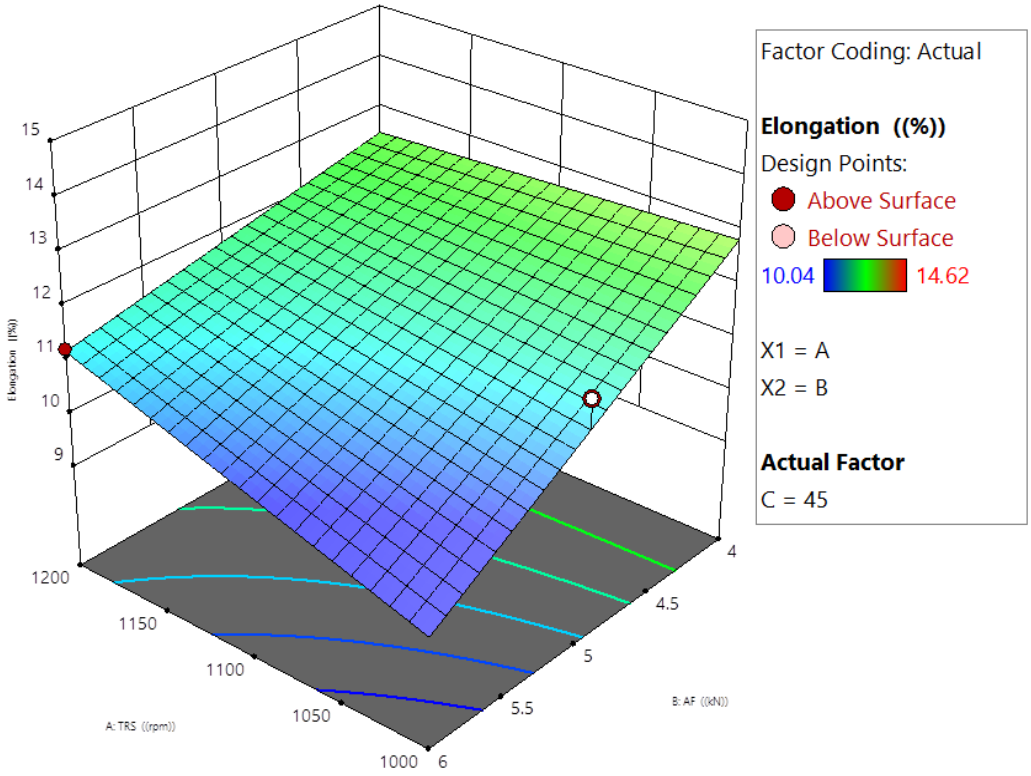

Figure 5(a). 3D surface plot between Elongation (%), AF and TRS.

Figure 4b shows the 3D surface plot between Tensile Strength, Welding speed and TRS. The tensile strength measurements exhibit a range from 110.64 MPa to 138.42 MPa. The intricate link between tensile strength, welding speed (C-WS), and tool rotational speed (A-TRS) during the welding process is depicted by the 3D response surface methodology (RSM) graphic. According to the visualization, tensile strength strongly depends on both factors, with the maximum values (140–150 MPa) taking place when low welding rates (30–36 mm/min) and high tool rotational speeds (about 1200 rpm) are combined. Tensile strength progressively drops as welding speed and tool rotation speed increase, reaching minimal values in the blue zone, which represents combinations of high welding speed and low rotational speed. This gradient effect is evident across the surface. This pattern indicates that processing parameters that limit the tool's linear advancement rate while permitting adequate heat generation and plastic flow enhance the material integrity.

Figure 5a presents the relationship between Elongation (%), Axial Force (kN) and Tool Rotation Speed (rpm). According to the surface, elongation rises with decreasing axial stresses (4-6 kN) and increasing tool rotation rates (1000-1200 rpm). Higher rotation speeds and lower axial forces seem to produce the best elongation values (about 14–15%). As the tool rotation speed increases and the axial force drops, the elongation % improves, as visible by the gradient. Elongation (%), Welding Speed (mm/min), and Tool Rotation Speed are shown in connection to each other in Figure 5b. Higher elongation values are obtained at moderate tool rotation speeds (about 1100–1150 rpm) in conjunction with lower welding speeds (approximately 30-36 mm/min), according to the surface. Higher welding rates result in a saddle-like surface pattern because the elongation drastically reduces, especially when paired with either extremely high or very low rotating speeds 25.

The connection between Elongation (%), Welding Speed (mm/min), and Axial Force (kN) is shown in Figure 5c. This surface demonstrates that lower welding speeds and lower axial forces work together to produce maximum elongation values (12–15%). The lowest elongation values occur at high welding speeds paired with high axial forces, and the elongation percentage steadily drops as both welding speed and axial force increase. All together these graphs indicate that less axial force (about 4-4.5 kN), a moderate to high tool rotation speed (1100-1200 rpm), and a lower welding speed (30-36 mm/min) would be the ideal settings to maximize the elongation % in this operation.

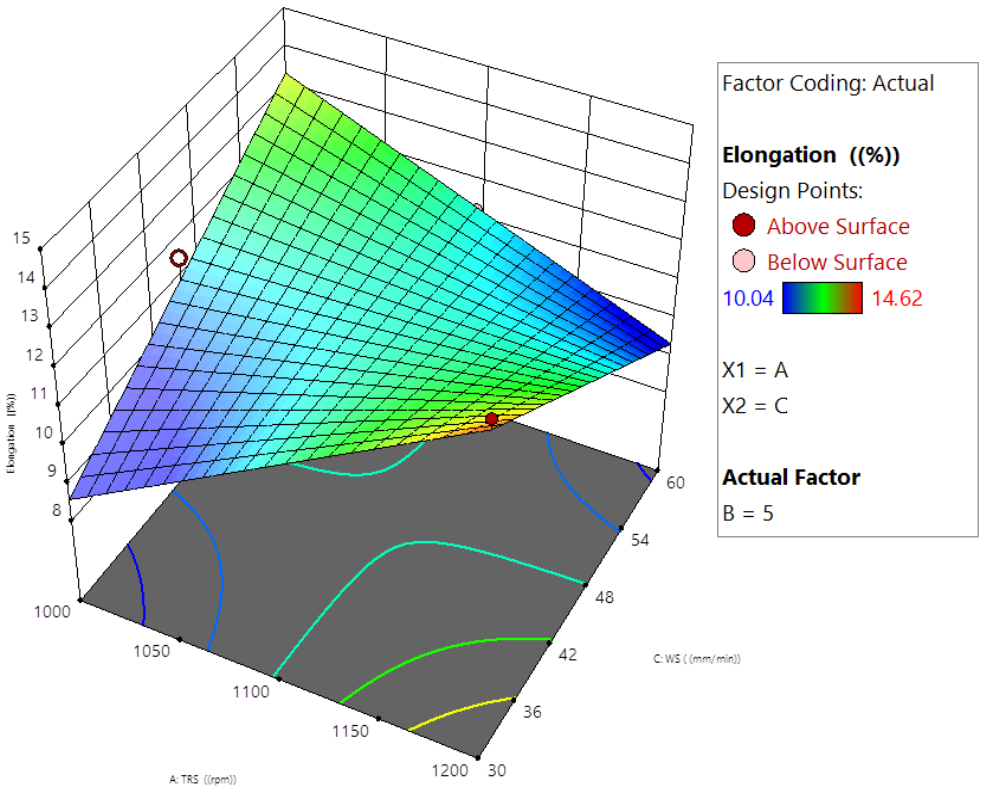

Figure 5(b). 3D surface plot between Elongation (%), WS and TRS.

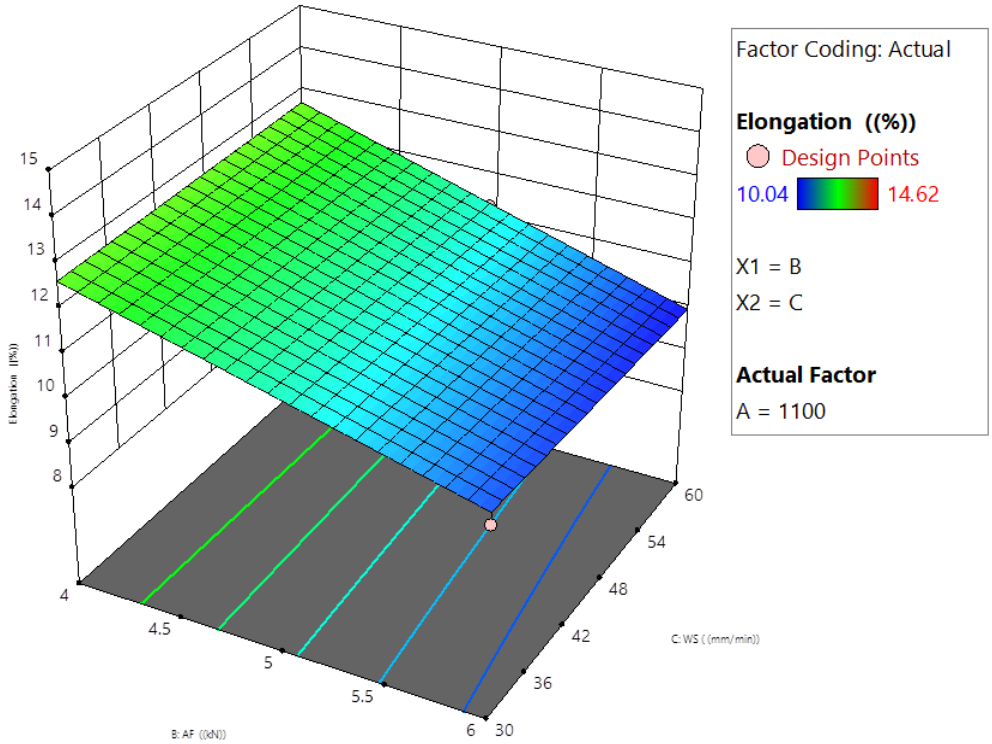

Figure 5(c). 3D surface plot between Elongation (%), WS and AF.

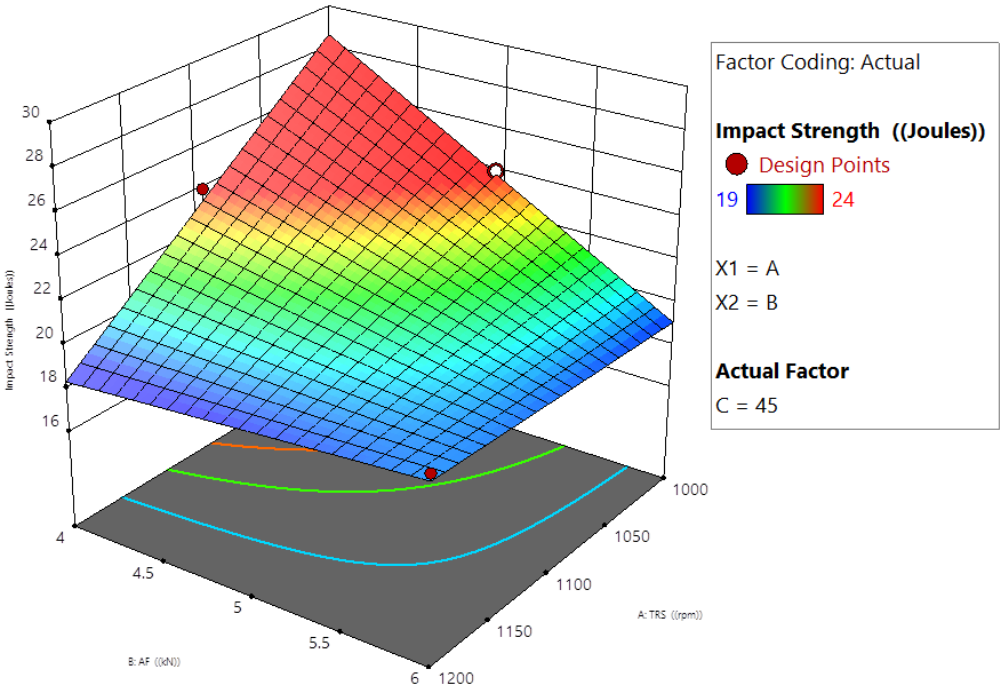

Figure 6(a). 3D surface plot for Impact strength with TRS and AF.

As axial force drops (from 6 to 4 kN) and tool rotation speed drops (from 1200 to 1000 rpm), Figure 6a shows that impact strength increases noticeably. The lowest axial force and rotation speed combination results in the highest impact strength values (28–30 J/cm²). This link most likely arises from the fact that lower rotation rates and axial forces produce less heat, which leads to finer grain structures and fewer weld zone flaws. Grain coarsening and thermal deterioration can result from excessive heat input from

increased axial forces and rotation rates, which reduces the material's ability to withstand impacts 16. As welding speed drops from 60 to 30 mm/min and tool rotation speed drops from 1200 to 1000 rpm, Figure 6b illustrates that impact strength rises. At the lowest values of both factors, the impact strength is at its best. The heat-to-mass ratio during welding is the source of this relationship; lower rotating rates avoid overheating and the ensuing microstructural damage, while slower welding speeds enable better mixing and consolidation of the material with less turbulence 17.

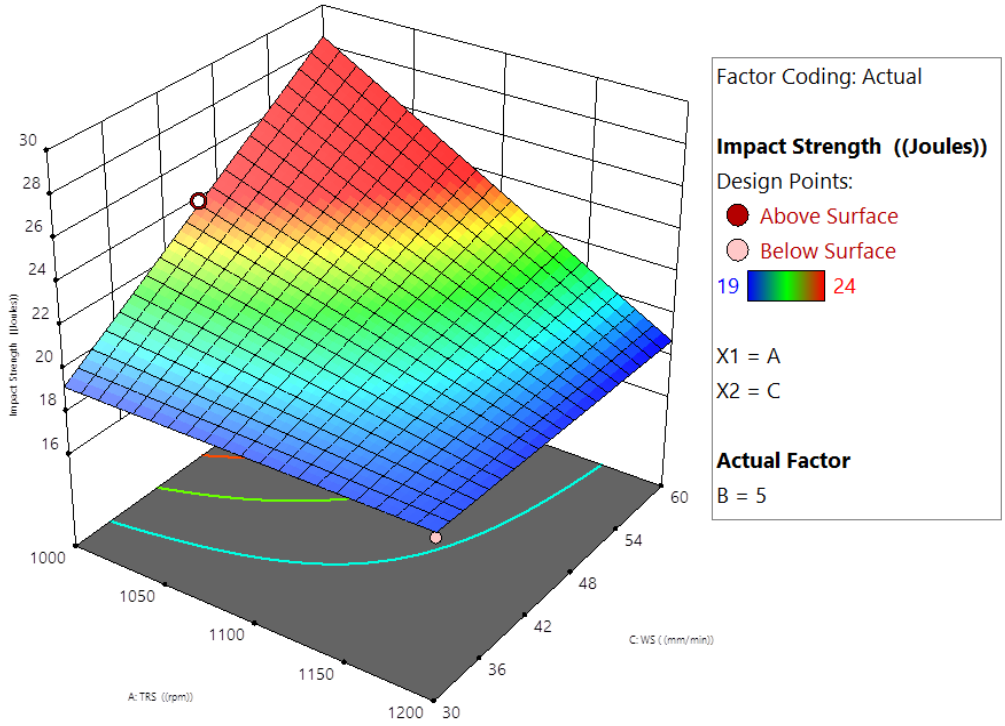

Figure 6(b). 3D surface plot for Impact strength with TRS and WS.

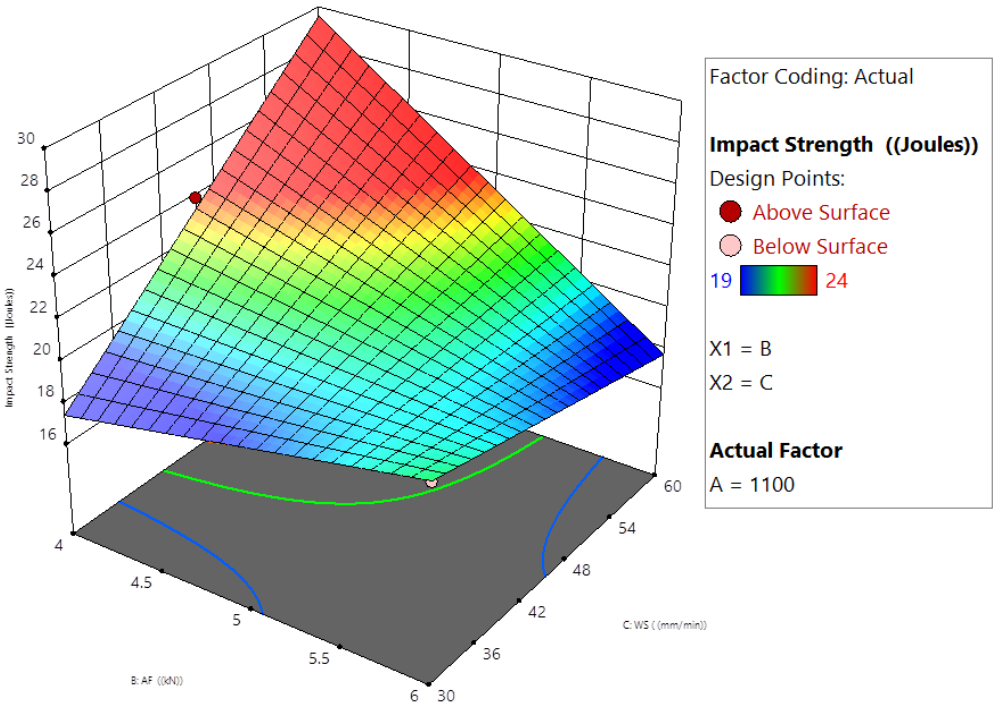

Figure 6(c). 3D surface plot for Impact strength with AF and WS.

Figure 6c shows that when the axial force and welding speed are at their lowest levels (30 mm/min and 4 kN, respectively), impact strength is maximized. Better material flow and less heat input work together to produce the mechanistic explanation. Slower welding speeds provide enough time for appropriate material intermixing and consolidation without undue thermal effects, while lower axial forces produce less heat from friction and less severe plastic deformation. By adjusting these variables, a balance is achieved where there is enough heat and plastic deformation to produce a strong weld without the negative consequences of too much heat input, which could cause coarse grains, precipitation dissolution, or thermal degradation, all of which would reduce the material's ability to withstand impacts.

With standard error values ranging from 0 to 8,000, Figure 7a shows a saddle-shaped response surface where micro hardness is optimum at moderate welding speeds (around 48 mm/min) in conjunction with lower axial forces (4-4.5 kN). Similar saddle-shaped pattern is shown in Figure 7b, although at higher values (1150–1200 rpm), the tool rotation speed has a greater impact on micro hardness. Contour lines show the intricate interactions between welding speed and rotation speed. With a markedly different pattern and an upward curvature toward higher axial forces and tool rotation speeds, Figure 7c suggests that the largest micro hardness error occurs at this combination. The steeper gradient along the rotation speed axis indicates the stronger influence of micro hardness error. When taken as a whole, these visualizations show how highly non-linear the correlations are between process parameters and micro hardness, with notable synergistic effects that cannot be anticipated by examining each parameter alone. While the different surface shapes between plots show that different parameter combinations require different optimization approaches to achieve desired micro hardness properties with minimal variability, the consistent appearance of optimal welding speed ranges (42-48 mm/min) across multiple parameter combinations offers helpful guidance for process optimization. Preceding Taguchi-FMS frameworks for machining efficiency are extended by the RSM-driven optimization of interfacial chemistry in welds, which now aims to minimize defects and maximize strength in multi-alloy joining systems [33-34].

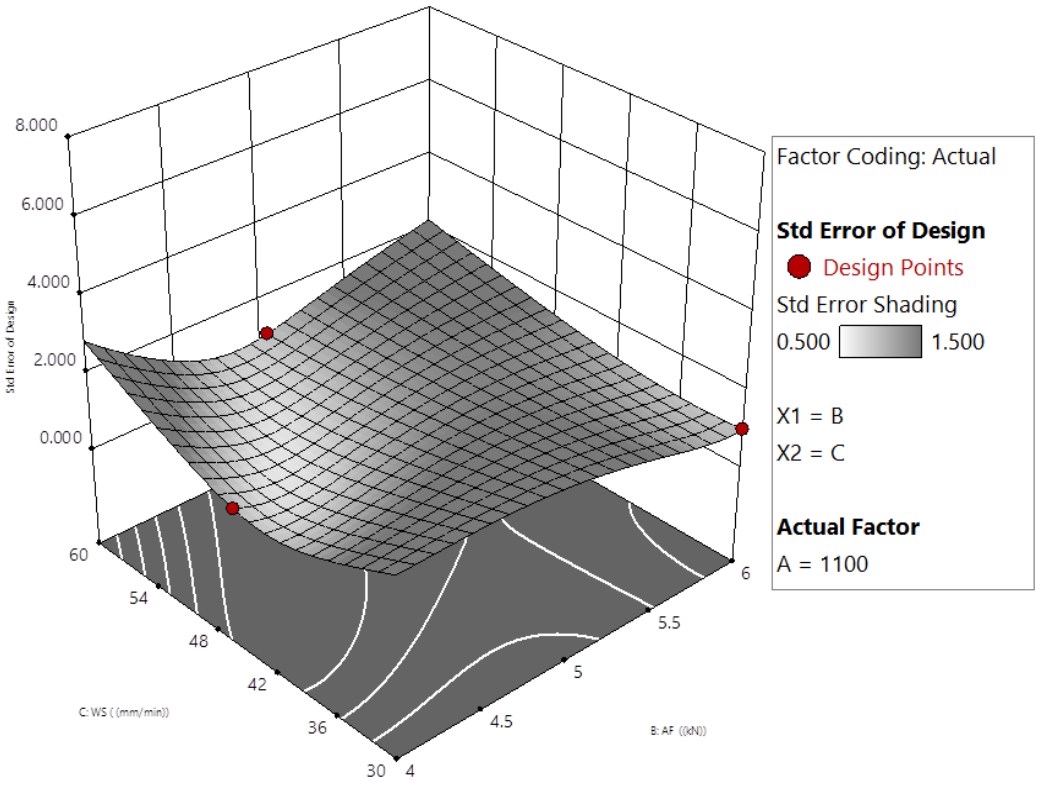

Figure 7(a). 3D surface plot between Micro Hardness, WS and AF.

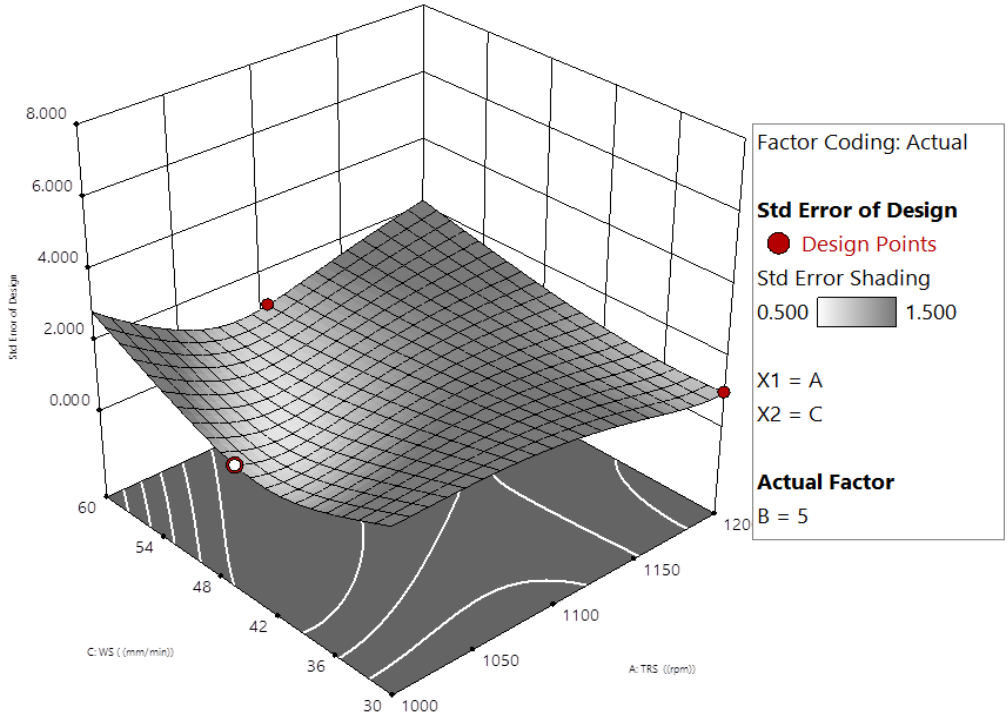

Figure 7(b). 3D surface plot between Micro Hardness, WS and TRS.

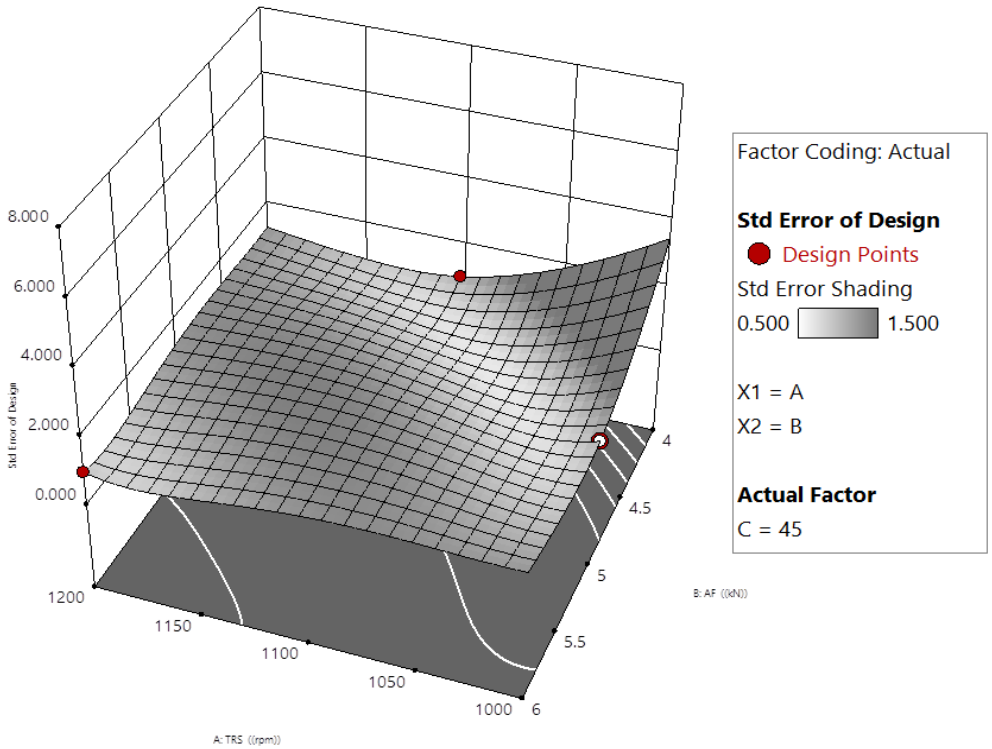

Figure 7(c). 3D surface plot for Micro Hardness between Micro Hardness, AF and TRS.

Mathematical Models

The equation used with actual factors enables scientists to predict responses by setting specific values for each factor. Each factor's specified levels need to be presented in their original unit values. Mathematical predictions using this equation should not measure a variable's relative contribution because degrees of freedom exist to match variable units yet the intercept point does not align with design space limits.

Impact Strength = 63.1111 + -0.0871429 * A + -20.3333 * B + 3.2127 * C + 0.0271429 * AB + -0.00161905 * AC + -0.257143 * BC

Tensile Strength =190.729 + 0.00555238 * A + -96.7867 * B + 6.7506 * C + 0.0716143 * AB + -0.00681524 * AC + 0.252952 * BC

Elongation = -35.8744 + 0.0475286 * A + -7.63667 * B + 1.82606 * C + 0.00607143 * AB + -0.00163238 * AC + -0.00695238 * BC

Micro Hardness = -397.9 + 0.38281 * A + 19.7 * B + 13.8968 * C + -0.000142857 * AB + -0.00981905 * AC + -0.619048 * BC

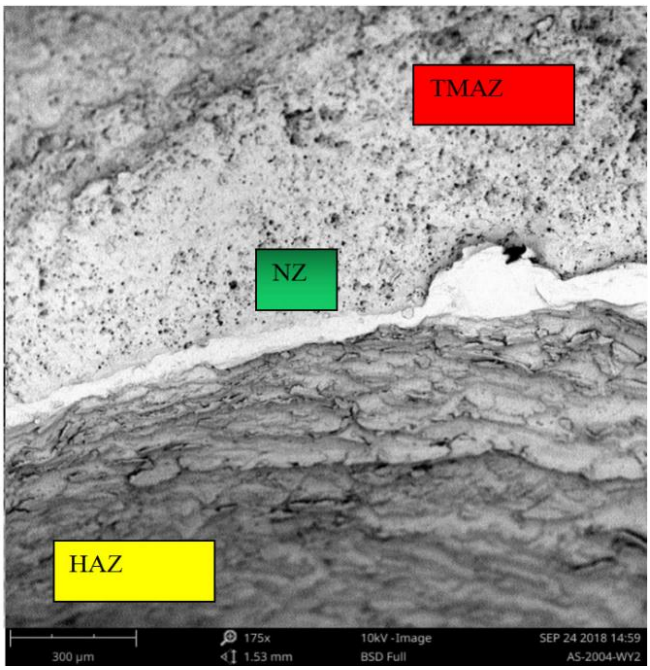

Figure 8. SEM of FSW specimen for 130 mm/min WS, 5 KN AF with 1200 rpm TRS.

Where

A = Tool Rotational Speed (TRS)

B = Axial Force (AF)

C = Welding Speed (WA)

Micro Structural Analysis

Figure 8 illustrates the microstructural analysis of FSW welded AA 7079 and AA 6063 joint, Heat Affected Zone (HAZ), Thermo-Mechanically Affected Zone (TMAZ), and Nugget Zone (NZ) three distinct zones are identified and shown. This SEM taken for the optimum process parameters of rotational speed of 1200 rpm, axial force of 5 kN, and welding speed of 130 mm/min. The SEM imaging was taken by using a JSM-IT500 SEM device, manufactured by JEOL Ltd., Japan, in 2018. Grain elongation and curvature in the Thermomechanical Affected Zone (TMAZ) result from material mixing, highlighting the impact of frictional heat and welding speed on the tensile properties.

The grain size in the Heat Affected Zone (HAZ) is slightly larger than that of the base metal. The augmentation of grain dimensions is significantly affected by the quantity of thermal energy produced throughout the welding procedure on the plate. Higher tool rotational speed generates more frictional heat that leads to an increased temperature in the weld zone. A greater amount of frictional heat develops from forcing the tool deeper into the material through increased axial force delivery. No specific axial force measurement provides the best outcome for maximum joint strength. The proper force within this specified range leads to proper material mixing while preventing damage to the weld zone. Welds with dense homogeneous microstructures develop when axial force application is done correctly leading to increased tensile strength.

CONCLUSION

In this work, the mechanical properties of friction stir welded dissimilar aluminum alloys AA 7079 and AA

6063 were successfully studied. The mechanical properties such as hardness, impact strength, tensile strength, and percentage of elongation. The highest mechanical strength of welded joints studied by optimizing welding speed (WS) along with axial force (AF) and tool rotation speed (TRS) by implementing Taguchi's L9 orthogonal array. The Response Surface Methodology analysis enabled researchers to find the ideal combination of these characteristics. The optimum combination for tensile strength and elongation has been realized in process parameters such as 30 mm/min welding speed, 5 KN axial force with tool rotation speed of 1200 rpm. The maximum of hardness value and impact strength is attained at the process parameters of 45 mm/min welding speed, axial force 4 KN while the tool rotated at the speed of 1100 rpm. The research outcome confirms that the welding operations with slower speeds and reduced force levels delivered better elongation and impact strength results but tool rotation at elevated speeds together with increased force levels tended to enhance tensile strength. A mathematical model is developed in this study; it serves as a forecasting tool to predict the FSW joint mechanical performance in relation to specific process parameters to improve industrial welding conditions. The investigation enlarges acquaintance the FSW process for dissimilar aluminum alloys by revealing methods to improve welding quality with extending the FSW welding process.

REFERENCES

1. Kwon, Y. J., Ichinori Shigematsu and Naobumi Saito (2008) Dissimilar friction stir welding between magnesium and aluminum alloys. *Materials Letters*, **62**, 23, 3827–3829.

2. Mishra, R. S., Ma, Z. Y. (2005) Friction stir welding and processing. *Mater. Sci. Eng. R Rep*., **50**, 1–78.

3. Chen, Y. C., Nakata, K., Liu and F. C. (2013) Friction stir welding of aluminum alloy to steel. *Mater. Des*. **45**, 135–140.

4. Zhang, H. J., Liu, H. J., Yu, L. (2011) Microstructure and mechanical properties of friction stir welded joints of AZ31 magnesium alloy. *Trans. Nonferrous Met. Soc*. *China*, **21**, 974–979.

5. Mehta, K. P., Badheka, V. J. (2016) Hybrid approaches of assisted heating and cooling for friction stir welding of copper to aluminum joints. *J. Mater. Process. Technol*., **239**, 336–345.

6. Patel, V. V., Badheka, V. J., Kumar, A. (2019) Effect of tool pin profiles on material flow and defect formation in friction stir welding of aluminum to steel. *J. Mater. Eng. Perform*, **28**, 1234–1244.

7. Kumar, N., Mishra, R. S., Yuan, W. (2020) Friction stir welding of aluminum to steel using WC-TiN coated tools. *J. Mater. Process. Technol.*, **275**, 116–123.

8. Mohammadi, J., Behnamian, Y., Mostafaei, A. and Gerlich, A. P. (2015) Tool geometry, rotation and travel speeds effects on the properties of dissimilar magnesium/aluminum friction stir welded lap joints. *Materialsand Design*, **75**, 95–112.

9. Kumar, S. D., Pugazhenthi, R., Danial, S. A. A. and Swaminathan, G. (2021) Optimization of Dissimilar aluminum alloy by Friction stir welding Process Control variables with Multiple Objectives. *In Journal of Physics. Conference Series*, **2040**, 1, 012042.

10. Yang, J., Oliveira, J. P., Li, Y., Tan, C., Gao, C., Zhao, Y. and Yu, Z. (2022) Laser techniques for dissimilar joining of aluminum alloys to steels. A critical review. *Journal of Materials Processing Technology*, **301**, 117443.

11. El-Sayed, M. M., Shash, A. Y., Abd-Rabou, M. and ElSherbiny, M. G. (2021) Welding and processing of metallic materials by using friction stir technique. A review. *Journal of Advanced Joining Processes*, **3**, 100059.

12. Elyasi, M., Taherian, J., Hosseinzadeh, M., Kubit, A. and Derazkola, H. A. (2023) The effect of pin thread on material flow and mechanical properties in friction stir welding of AA6068 and pure copper. *Heliyon*, **9(4)**.

13. Wu, X., Zhang, C., Wang, Z., Zhao, X., Yao, H., Li, Y. and Jiang, F. (2024) Experimental research on the welding strength of PCBN and cemented carbide materials for cutting tools application. *International Journal of Refractory Metals and Hard Materials*, **119**, 106528.

14. Singh, K., Singh, G. and Singh, H. (2023) The influence of holding time on the characteristics of friction stir welded dissimilar magnesium alloy joints during post welding heat treatment. *Proceedings of the Institution of Mechanical Engineers, Part L. Journal of Materials. Design and Applications*, **237(1)**, 170–182.

15. Prabhakar, D. A. P., Shettigar, A. K., Herbert, M. A., GC, M. P., Pimenov, D. Y., Giasin, K. and Prakash, C. (2022) A comprehensive review of friction stir techniques in structural materials and alloys. Challenges and trends. *Journal of materials research and technology*, **20**, 3025–3060.

16. Scialpi, A., De Filippis, L. A. C., Cavaliere, P. (2021) Influence of tool material on the wear

behavior of PCBN tools in friction stir welding of high-strength alloys. *Wear*, **477**, 203–210.

17. Zhang, Z., Liu, H. J., Li, J. (2020) Effect of post-weld heat treatment on the microstructure and mechanical properties of friction stir welded aluminum-titanium joints. *Mater. Sci. Eng.* A, **772**, 138–145.

18. Liu, X., Zhang, Y., Li, X. (2021) Effect of post-weld heat treatment on the fatigue performance of friction stir welded aluminum-magnesium joints. *Int. J. Fatigue*, **143**, 105–112.

19. Khalafe, Wazir Hassan, Ewe Lay Sheng, Mohd Rashdan Bin Isa, Abdoulhadi Borhana Omran and Shazarel Bin Shamsudin. (2022) The effect of friction stir welding parameters on the weldability of aluminum alloys with similar and dissimilar metals. *Metals*, **12(12)**, 2099.

20. Chinnasamy, S. and Arunachalam, A. (2023) Experimental investigation on direct expansion solar-air source heat pump for water heating application. *Renewable Energy*, **202**, 222–233.

21. Chinnasamy, S., Prakash, K. B., Kalidasan, B. and Sampathkumar, A. (2024). Solar-air source heat pump water heater for scorching climatic condition: energy, exergy, economic and enviro economic (4E) exploration for sustainable future. *Applied Thermal Engineering*, **240**, 122212.

22. Chinnasamy, S., Prakash, K. B., Kalidasan, B. and Sampathkumar, A. (2024) Optimal utilisation of low-grade solar-air source for heat pump water heating using a dual-source evaporator with forced convection. *International Communications in Heat and Mass Transfer*, **150**, 107174.

23. Bhatnagar, Shaurya, Gaurav Kumar, Husain Mehdi and Mukesh Kumar (2023) Optimization of FSW parameters for enhancing dissimilar joint strength of AA7050 and AA6061 using response surface methodology (RSM). *Materials Today. Proceedings*.

24. Prabhakar, D. A. P., Arun Kumar Shettigar, Mervin A. Herbert, Manjunath Patel, G. C., Danil Yu Pimenov, Khaled Giasin and Chander Prakash (2022) A comprehensive review of friction stir techniques in structural materials and alloys. Challenges and trends. *Journal of Materials Research and Technology*, **20**, 3025–3060.

25. Zhou, L., Li, G. H., Zha, G. D., Shu, F. Y., Liu, H. J. and Feng, J. C. (2018) Effect of rotation speed on microstructure and mechanical properties of bobbin tool friction stir welded AZ61 magnesium alloy. *Science and Technology of Welding and Joining*, **23**(**7**), 596–605.

26. Çam, Gurel, Vahid Javaheri and Akbar Heidarzadeh (2023) Advances in FSW and FSSW of dissimilar Al-alloy plates. *Journal of Adhesion Science and Technology*, **37(2)**, 162–194.

27. Arora, Kanwer S., Sunil Pandey, Michael Schaper and Rajneesh Kumar (2010) Effect of process parameters on friction stir welding of aluminum alloy 2219-T87. *The International Journal of Advanced Manufacturing Technology*, **50**, 941–952.

28. Kumar, Rahul, Avinash Lakshmikanthan, Priyaranjan Sharma and Sanjay D. Nikhade (2025) A critical review of material flow investigation in friction stir welding using novel techniques. *Journal of Adhesion Science and Technology*, 1–32.

29. Yaduwanshi Deepak Kumar, Chennu Rama Mohan Rao, Ramana Murty Naidu, S. C. V., Sanjay G. Sakharwade, Sumit Sharma, Khalkar, V., Baskar, S. and Gopal Kaliyaperumal (2024) Thermal evaluation of aluminum welding: a comparative study of friction stir welding (FSW), plasma-fsw, and tungsten inert gas (TIG)-FSW techniques. *International Journal on Interactive Design and Manufacturing (IJIDeM)*, **18(8)**, 5501–5513.

30. Kumaraswamy, J., Vijaya Kumar, Purushotham, G. ( ) Evaluation of the microstructure and thermal properties of (ASTM A 494 M grade) nickel alloy hybrid metal matrix composites processed by sand mold casting. *International Journal of Ambient Energy*, **42**, 1–10.

31. Raja, T., Devarajan, Y., Jayasankar, P., Singh, D., Subbiah, G. and K. L. (2024) Characterization and sustainable applications of galinsoga parviflora natural fibers. A pathway to eco-friendly material development. *Results in Engineering*, **24**, 103601.

32. Sakthimurugan, V., Yuvarajan, D., Ganesan, S., Upadhye, V. J., Gill, A. and kailiappan, N. (2025) Investigation on Influence of Acetylene Enrichment in Diesel Engines Operating with Microalgae-Waste Plastic Oil-Heptane Fuel Mixture. *Energy Science & Engineering*.

33. Arul, M., Subramaniyan, C., Sakthivelmurugan, E. And Sureshkumar, M. (2024) Optimising mechanical properties of epoxy matrix hybrid composites through sic filler integration and fiber reinforcement: The Taguchi approach. *Cellulose Chemistry & Technology*, **58**.

34. Subramaniyan, C., Prakash, S. V., Bhuvanesh, N., Kalidasan, B. and Amarkarthik, A. (2021) Study based on the reduction of lot time by implementing set production and FMS in the traditional batch production system. *Materials Today: Proceedings*, **45**, 502–506.